Strontium clusters: Many-body potential, energetics, and structural transitions

Guan Ming Wang, Estela Blaisten-Barojas,[a] and A. E. Roitberg
School of Computational Sciences, George Mason University, Fairfax, Virginia 22030

T. P. Martin
Max-Planck-Institut für Festkörperforschung, Stuttgart, Germany

(Received 3 April 2001; accepted 17 May 2001)

A many-body potential for strontium clusters is developed with parameters fitted to the energy surface of strontium clusters containing up to ten atoms calculated within the density functional theory in the generalized gradient approximation. Structure and energetics of the most stable cluster isomers with up to 63 atoms are obtained with genetic algorithms. Additionally, the high resolution mass spectrum of strontium clusters up to Sr_{96} at finite temperature is provided. Several thermodynamic properties are studied under the many-body potential as a function of temperature. It is found that stability patterns, indicating how stable a cluster size is with respect to its neighboring sizes, change significantly with temperature. This behavior is due to structural transitions of the strontium clusters that occur at finite temperatures. A comparison with the experimental mass abundance indicates that only the structures above 400 K were observed experimentally. Very prominent magic numbers are predicted at 34 and 61. © *2001 American Institute of Physics.* [DOI: 10.1063/1.1384454]

I. INTRODUCTION

Scientists in physics, chemistry, and material science have recently become interested in the exotic properties displayed by atomic clusters at finite temperatures.[1,2] At zero temperature, the ground state structure of an atomic cluster is a geometry associated with the isomer having the lowest potential energy. The search for the global minimum of a function that has many variables and multitude of local minima is a difficult problem encountered in many fields. At finite temperatures the complexity of the problem increases since low-lying local minima play an increasingly important role in determining the structural stability[3] and temperature dependent structural transitions are to be expected. Until very recently the model systems used to investigate such transitions, both theoretically and experimentally, have been inert gas and alkali metal clusters. However, the alkali metals are not representative for the whole class of metallic elements. Our investigation is aimed at introducing the next stage of difficulty by working with less simple metals, the alkaline earths, in particular, strontium.[4–6]

Alkaline earth metals are of interest because the structural behavior of the bulk is unconventional. These elements display hexagonal closed packed (hcp)→faced centered cubic (fcc)→body centered cubic (bcc) crystalline structure with increasing atomic number. In addition, strontium undergoes a structural transiton fcc→bcc at 3.5 GPa.[7] Not many studies exist for strontium clusters. At the *ab initio* level there are calculations within LDA for Sr_2,[8] and selected geometries of Sr_3 through Sr_{13}.[9] Hearn and Johnston[10] fitted the parameters of the Murrell-Mottram (MM) potential[11] on bulk strontium elastic properties and reported a series of cluster structures up to Sr_{20} generated under this potential. From the experimental perspective, there are spectroscopic measurements for the dimer,[12] mass spectra for up to Sr_5 (Ref. 13) and larger strontium clusters[14,15] showing that the magic numbers are substantially different than those of Lennard-Jones clusters. The binding energy for Sr_2 has been measured,[12] although the energetics of larger clusters has not been studied in the laboratory.

In this paper we develop a many-body model potential for strontium clusters and fit its parameters to first principles calculations of Sr_2 to Sr_{10} clusters as well as to the elastic constants, cohesive energy, lattice constant and surface energy of the bulk. This potential follows an approach similar to that already developed for other metals.[3,16] With this potential we determine the global minimum structure of clusters up to Sr_{63}. In the process of obtaining the global minima with genetic algorithms[17] we generate many local minima that are collected and become part of this study as well. The experimental section includes the high resolution mass spectrum of hot strontium clusters. Making use of several of the calculated higher energy minima we study possible structural transformations for clusters of several sizes. This leads to a study of the stability of clusters at finite temperatures which is compared with the mass spectrum. Other cluster properties such as free energy, entropy, specific heat, and vibrational spectra are also part of this work.

II. MANY BODY POTENTIAL FOR STRONTIUM

As the other alkaline earths, strontium clusters have the characterisitic of growing from a van der Waals dimer that gains binding by adding atoms. Clusters are expected to attain the metallic properties of the bulk when they reach a

[a]Electronic mail: blaisten@gmu.edu

certain finite size, although this size might be quite large.[15,18] However, bulk fcc strontium has a peculiar electronic behavior since the density of states presents a small gap, being the Fermi energy precisely in the gap.[19] For that reason, until better calculations will be available, strontium is believed to be a semimetal at atmospheric pressures. At high pressures strontium becomes a bcc metal with no gap in the density of states.[7,20] It is therefore important to study the structural characterisitics for this type of material.

Two model potentials have been used in the literature to predict properties of bulk strontium. One is the pairwise additive Morse potential parametrized by Wales, Munro, and Doye[21] and the other is the MM potential[11] parametrized by Hearn and Johnston[10] that includes three-body terms. Both of these potentials could potentially be used to describe strontium clusters, although the parametrization was done on bulk properties. In fact clusters generated from both potentials have been reported. In the case of the Morse potential, clusters with polytetrahedral components tend to be priviliged,[22] whereas in the case of the MM potential, the icosahedral growth dominates.[10]

In this section we describe the parametrization scheme adopted for strontium clusters to generate the many-body potential based on the second moment approximation (SMA) (Refs. 23, 24) in its modified version for clusters.[16] The expression for this potential is as follows:

$$E_N=\sum_{i=1}^{N}\left\{\epsilon(N)\sum_{j\neq i}^{N}\exp\left(-p\left[\frac{r_{ij}}{r_0(N)}-1\right]\right)-\xi(N)\sqrt{\sum_{j\neq i}^{N}\exp\left(-2q(N)\left[\frac{r_{ij}}{r_0(N)}-1\right]\right)}\right\}, \quad (1)$$

where

$$F(N)=(F_{\mathrm{dimer}}-F_{\mathrm{fcc}})\left(\frac{2}{N}\right)^{X_F}+F_{\mathrm{fcc}}, \quad (2)$$

where F is either ξ, ϵ, r_0, or q. Five parameters (p and the four F_{fcc}) were fitted on experimental bulk properties: cohesive energy $=-1.73$ eV and lattice constant $=6.08$ Å,[25] surface energy $=0.41$ eV/atom,[26] elastic constants $c_{11}-c_{22}=9$ GPa, and $c_{44}=10$ GPa.[27] The errors of this fit were 0.35%, 0.1%, 0.1%, 7%, and 8.6%, respectively.

To fit the remaining 8 parameters (four F_{dimer} and four X_F) we performed first principles total energy calculations for Sr_2 through Sr_{10} within a hybrid approach of density functional generalized gradient approximation (GGA) (Ref. 28) with a Hartree–Fock description for the exchange energy.[29] A core-polarization potential was used to simulate the core electrons together with a 2-valence-electron pseudopotential and the SDD basis set with p and d polarization functions.[30] The GAUSSIAN 98 package[31] with B3PW91 was used throughout this work. Table I lists the geometry and binding energy of the clusters. The previous-to-last column of this table gives the number of points in each of the energy surfaces used in the fit of the potential parameters. All energies were converged to the eighth decimal place during the self consistent field loop. The minimization process was not constrained to keep a specific point symmetry. For comparison, Table I contains the binding energy of a comparable calculation published during the course of this study.[9] Our calculation of the binding energy is in excellent agreement with these results for sizes up to Sr_8. For Sr_9 and Sr_{10} we predict more bounded clusters. We also predict systematically shorter bond lengths for the smaller clusters due to the better description of the exchange energy.[18] Additionally, Ref. 9 does not provide information on points of the energy surfaces of the various clusters other than their minima.

TABLE I. Binding energies per atom and average bond length of S_2 through S_{10} calculated within GGA. Last two columns list the number of points of the potential energy surface used in the fitting of the parameters of Eq. (1) and binding energies from Ref. 9.

		E_N/N (eV/atom)	r_{ave} (Å)	No. points	E_N/N (eV/atom) Ref. 9
Sr_2	$D_{\infty h}$	0.0698	4.60	20	0.066
Sr_3	D_{3h}	0.2049	4.33	6	0.245
Sr_4	T_d	0.3958	4.17	8	0.481
Sr_5	D_{3h}	0.4426	4.20	12	0.512
Sr_6	C_{2v}	0.4821	4.20	20	0.553
Sr_7	D_{5h}	0.5763	4.18	15	0.680
Sr_8	C_s	0.5884	4.20	62	0.688
Sr_9	C_s	0.6296	4.20	27	0.587
Sr_{10}	C_{3v}	0.6455	4.22	12	0.590

The four parameters F_{dimer} and the four parameters, X_f were fitted on 20 points of the dimer energy curve and on 162 points corresponding to the energy surfaces of Sr_3 through Sr_{10} as indicated in Table I. The 13 parameters of the potential are: $\epsilon_{\mathrm{fcc}}=0.015\,761$ eV, $\xi_{\mathrm{fcc}}=0.3832$ eV, $r_{\mathrm{fcc}}=4.301$ Å, $q_{\mathrm{fcc}}=1.1132$, $p=17.649$, $\epsilon_{\mathrm{dimer}}=0.018\,089$ eV, $\xi_{\mathrm{dimer}}=0.139\,77$ eV, $r_{\mathrm{dimer}}=5.6$ Å, $q_{\mathrm{dimer}}=6.0$, $X_\xi=0.8$, $X_\epsilon=0.52588$, $X_{r_0}=3.6$, $X_q=0.65$. The error for the fit was 0.15 eV, which is less than 4%.

III. MODIFIED GENETIC ALGORITHM

Several methods for finding the global minimum of the potential energy surface (PES) have been proposed over the years for optimization of cluster geometries. Such optimization is difficult because the number of local minima increases exponentially with the number of atoms in the cluster.[32] The main problem associated with optimization is the tendency to be trapped in regions of the PES close to local minima that may be far from the global minimum. One of the earliest methods introduced to resolve this difficulty is simulated annealing[33] which requires jumps over energy barriers, a kinetic factor that hampers the search. Lower energy barriers may be obtained by smoothing the PES.[34] However, a drawback of smoothing techniques is that the global minimum of the modified PES might not be the same as that of the original PES. An alternative method is the basin-hopping algorithm[35] in which the PES is replaced by a modified surface containing only the basins of all known minima. Since each point in the catchment basin of a local minimum is assigned the energy of that minimum, this transformation obviously eliminates the barriers between adjacent minima. This modified PES is known as the inherent structure[36] and

the basin-hopping algorithm consists of a Monte Carlo search on this modified PES. A very different class of optimization methods are the genetic algorithms (GA) based on Darwinian evolution theory. In these methods several low energy structures are evolved by using operators reminiscent of the way nature splits and mutates parent genomes to produce offspring.[37,38] Applications to clusters have been published by several groups.[17,39–42]

In this work we apply a GA that evolves by performing the genetic operations on the PES represented by the inherent structure instead of the actual PES. A Lamarckian evolution is achieved because the GA combines only preselected points on the PES, those representing isomers corresponding to local minima, instead of combining arbitrary selected points on the PES.[43] Specifically, in our implementation of a Lamarckian GA, each individual is a random structure of an N-atom cluster which is loosely minimized to a local minimum. The coordinates of that minimum are the genes of that individual. A population in a given generation is defined as a group of such individuals. The energy of each minimum (E_i) is computed based on Eqs. (1)–(2) and the normalized fitness for that individual (f_i) is defined as

$$f_i = \frac{E_{\max} - E_i}{E_{\max} - E_{\min}}, \tag{3}$$

where $E_{\max}$ and $E_{\min}$ are the highest and lowest energies of the minima in the population. A GA iteration consists of the following. The initial population contains M minimized structures ranked in decreasing order according to their fitness. This describes the first generation. Three genetic operations are performed on the members of the present population to yield the subsequent generation: crossover, average, and elite. Two children are generated from two parents chosen at random from the M minimized structures by a multiple point crossover[44] in which each coordinate of one parent is exchanged by one coordinate of the other parent with probability p. The average operator creates one child by selecting at random two parents from the population and arithmetically averaging their coordinates. Subsequently, the structures generated with these two rules are locally minimized. The elite operation stipulates that some of the fittest individuals of the present population are passed intact to the next generation. The second population is formed by the M new individuals (local minima) that have higher fitness. The process is repeated until the lowest energy minimum found does not change over several generations. At this point the first GA iteration ends and the optimization is started again for a second iteration from a different initial population. The values $M=40$, $p=0.22$, and elite=18% ensured the most efficient optimization. For each cluster size, 100 iterations were performed. Contributions of the genetic operation known as mutation were proven to be insignificant in the genetic evolution of our system and therefore this operator was not applied. The major improvement of the Lamarckian-GA applied to our system is that the individuals correspond to local minima of the PES (cluster isomers), and therfore their fitness is high.

TABLE II. Binding energies per atom, average bond length, and type of structure of clusters containing up to 63 strontium atoms obtained with the many-body potential.

N	E_N/N	r_{ave}(Å)	Structure	N	E_N/N	r_{ave} (Å)	Structure
10	0.646	4.23	M LJ SC	37	0.934	4.29	SC
11	0.668	4.24	M LJ SC	38	0.943	4.30	LJ SC
12	0.693	4.23	M LJ SC	39	0.948	4.30	LJ
13	0.725	4.26	M LJ SC	40	0.951	4.30	LJ SC
14	0.732	4.28	M LJ SC	41	0.955	4.30	LJ
15	0.747	4.28	LJ SC	42	0.960	4.30	LJ SC
16	0.759	4.26	M LJ SC	43	0.966	4.30	LJ SC
17	0.770	4.27	LJ SC	44	0.967	4.30	LJ SC
18	0.782	4.29	M LJ	45	0.974	4.30	Ref. 16
19	0.801	4.30	M LJ SC	46	0.981	4.31	LJ SC
20	0.809	4.29	M LJ SC	47	0.984	4.30	LJ SC
21	0.816	4.31	SC	48	0.989	4.30	LJ
22	0.825	4.31	M LJ	49	0.995	4.30	LJ SC
23	0.838	4.28	M LJ	50	0.998	4.30	LJ
24	0.843	4.28	Ref. 16	51	1.003	4.29	SC
25	0.851	4.28	SC	52	1.009	4.29	LJ SC
26	0.860	4.28	M LJ	53	1.014	4.30	LJ
27	0.867	4.31	LJ	54	1.019	4.30	M LJ SC
28	0.876	4.30	SC	55	1.024	4.30	LJ SC
29	0.881	4.29	SC	56	1.025	4.30	LJ SC
30	0.889	4.30	SC	57	1.025	4.30	LJ SC
31	0.896	4.29	SC	58	1.029	4.31	LJ SC
32	0.904	4.31	LJ SC	59	1.031	4.30	LJ
33	0.909	4.29	SC	60	1.035	4.30	LJ SC
34	0.914	4.31	LJ	61	1.038	4.30	LJ SC
35	0.922	4.30	SC	62	1.040	4.30	LJ
36	0.928	4.31	LJ SC	63	1.043	4.30	LJ

IV. STRONTIUM CLUSTERS: STRUCTURE AND ENERGETICS

Strontium clusters containing up to 63 atoms were optimized with our GA procedure under the many body potential described by Eqs. (1)–(2). The binding energies of the global minimum structures are listed in Table II. Each cluster in our set of most stable isomers has a structure that can be found in one of the sets produced using prototype potentials such as the Lennard-Jones (LJ),[45] the Sutton-Chen 12-6 (SC),[46] and Morse (M).[22] The type of strucure is listed in the table. Most of these structures have local hcp, icosahedral, and decahedral motifs. Sr_{24} and Sr_{45} were identified as global isomers for the rhodium clusters.[16] The most stable structures of Sr_{13} and Sr_{55} are Mackay icosahedra; Sr_{38} is the truncated octahedron. At other cluster sizes, hcp and fcc motifs can be identified. For example, Sr_{26} and Sr_{48} are clusters cut from the hcp lattice. The average bond distance as a function of cluster size is also reported in Table II. Although the dimer has a large interatomic separation, the bond distance rapidly contracts to 4.17 Å for Sr_4 and expands again with increasing cluster size reaching 4.3 Å at about $N=20$, which is already the nearest neighbor distance of bulk fcc strontium. In Fig. 1 we give a comparison between our results of the binding energies per atom (black dots) and those obtained using the MM (Ref. 10) (triangles) and Morse[22] (squares) potentials for strontium. The MM potential overestimates the binding energy by about 20% whereas the Morse potential underestimates the binding energies by 10%–20% when comparing to our GGA and many-body results. Additionally, for several

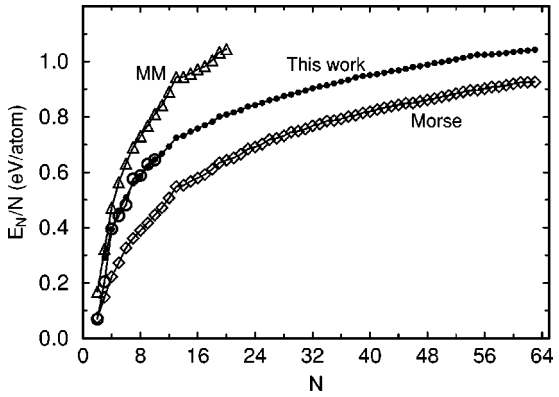

FIG. 1. Comparison of binding energy as a function of cluster size: this work GGA calculation (circles), the many-body potential (black dots), MM potential Ref. 10 (triangles), Morse potential Ref. 21 (diamonds).

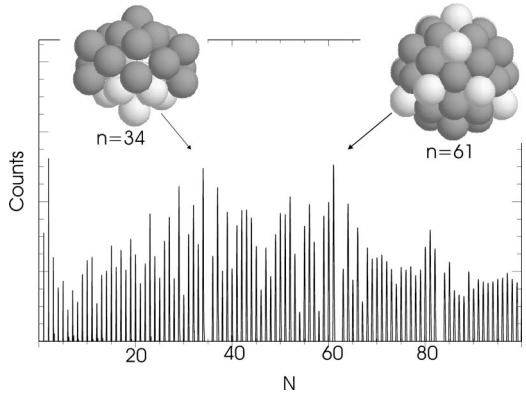

FIG. 2. Mass spectrum of strontium clusters.

sizes the MM structures are different such as $N=8$, $N=15$ through $N=18$. Only a few Morse structures for the small clusters coincide with ours as seen in Table II.

V. MASS SPECTRUM OF STRONTIUM CLUSTERS

Strontium clusters were produced in a low-pressure, inert gas, condensation cell. The metal was heated in a tantalum crucible producing a vapor that was quenched in 1 mbar of helium gas cooled to 100 K. Strontium clusters condensed out of the cooled vapor and were entrained in the flow of helium gas as it passed through various stages of differential pumping into the acceleration region of a time-of-flight mass spectrometer. Before pulsed extraction at a right angle into the drift tube, the clusters were ionized and heated with laser pulses. The wavelength of the lasers used in this experiment must be chosen carefully as described below.

The clusters produced in this experiment had a broad, smooth size distribution peaked at about 1000 atoms. It was necessary to heat the clusters to a temperature at which massive evaporation took place for two reasons. First, only through evaporation could magic sizes be induced in the size distribution. Clusters with these magic sizes resisted evaporation indicating that they were unusually stable. Second, only by evaporation could a large enough number of small (less than 100 atoms) clusters be produced to provide acceptable count rates. Laser light was also used to ionize the clusters. However, they should acquire a charge of only $+1$. Further ionization would complicate the interpretation of the mass spectrum. Therefore, one laser can be used for both heating and ionization only if the laser has a photon energy near the first ionization threshold of the clusters. This would allow the use of a high laser fluence necessary for heating without resulting in multiple ionization. Alternatively, two lasers could be used; a low fluence, short wavelength laser for ionization, and a high fluence, long wavelength laser for heating. Both types of experiments were carried out yielding the same results. The one-laser experiment used 400 nm light and the two-laser experiment used both 532 nm and 308 nm photons.

Mass spectra of strontium clusters have been shown to demonstrate very pronounced icosahedral structure, but only between 550 and 900 atoms. The detailed subshell structure observed in this limited size range is identical to that seen and reported for Mg and Ca clusters. The structure corresponds to the formation of the 5th shell as each of the 20 triangular facets of the icosahedron is covered with atoms. This result was reported and discussed in detail.[6] That portion of the same spectrum for clusters containing less than 100 atoms was neither reported nor understood at the time, but is now shown in Fig. 2. A similar spectrum has been reported in Ref. 15.

The mass spectrum of Sr_N clusters, Fig. 2, contains strong mass peaks at, for example, $N=34$ and 61, thus identifying particularly stable clusters. The high stability of these clusters will be associated with their structure rather than with the number of valence electrons. Since such an interpretation differs from that of well-studied alkali metal clusters, a few words of explanation are in order. If an alkali metal cluster is heated to a temperature high enough to cause massive evaporation on a time scale of 10^{-8} s, the cluster can be viewed as a more-or-less spherical liquid droplet. All of these clusters look the same. Magic sizes are marked by the filling of highly degenerate electronic subshells of electrons. Alkaline earth clusters sublime at these high temperatures. That is, the clusters are solid at the temperatures necessary for evaporation. Therefore, it is more meaningful to speak of their structure.

The spectrum also shows deep minima at $N=35$, 62, and 83, identifying particularly unstable clusters. The minima are found immediately after maxima because an extra atom added to a stable closed structure often has a low coordination with the rest of the cluster. It is the strong peaks for $N=34$ and 61 that are at the focus of the present study.

VI. STRUCTURAL TRANSITIONS AT FINITE TEMPERATURE

Results described in Secs. II–IV are for zero temperature. On the other hand, the experimental results of Sec. V were obtained at finite temperatures. Therefore, we investigated the possibility that clusters would change structure at finite temperatures. Indeed they do. Using Monte Carlo, Molecular Dynamics simulations[16] and the GA results, stable isomers with energies within 1 eV above the global minimum were collected for each cluster size. Once the frequen-

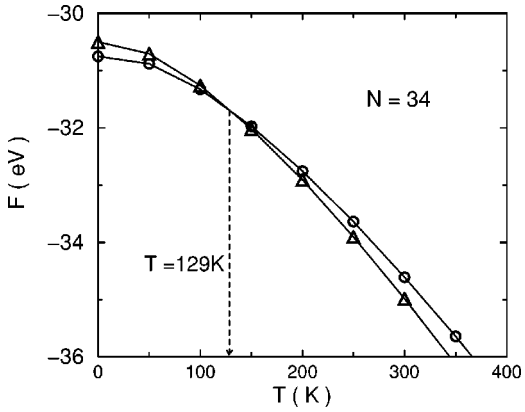

FIG. 3. Vibrational free energy as a function of temperature of two isomers of Sr_{34}: global minimum C_{2v} (circles) and higher energy isomer D_{5h} (triangles).

cies of the normal modes of vibration of all these local minima were calculated, the vibrational free energy of the clusters as a function of temperature can be estimated in the harmonic approximation. The calculation is done in the canonical ensemble assuming that each isomer is in thermal equilibrium. For example, Fig. 3 illustrates the vibrational free energy as a function of temperature for two isomers of Sr_{34} with symmetries C_{2v} and D_{5h}. The C_{2v} structure is the global minimum, the D_{5h} is one of the higher energy isomers within the 1 eV window above the global minimum. The free energy of this particular isomer crosses C_{2v} free energy at a lowest temperature T_s. Although many more isomers, other than the D_{5h}, lay within the energy window above the global minimum, their free energies either cross the free energy of the global at temperatures higher than T_s, or do not cross at all for temperatures below 500 K. For Sr_{34} at finite temperatures, the D_{5h} structure is therefore more stable than the global minimum C_{2v} isomer. Depicted in Fig. 4 is the internal energy of Sr_{34} clearly showing at $T_s = 129$ K the change of structure from the low temperature C_{2v} isomer to the D_{5h} isomer at temperatures above T_s.

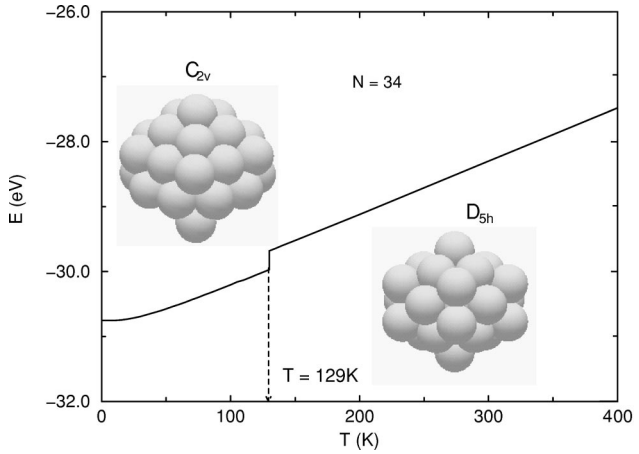

FIG. 4. Internal energy of Sr_{34} as a function of temperature. The global minimum C_{2v} is depicted at low temperatures. The higher energy isomer D_{5h} is depicted at higher temperatures.

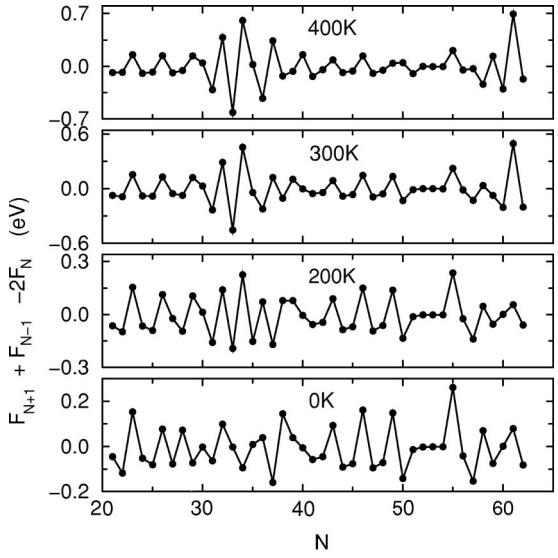

FIG. 5. Second difference of the vibrational free energy vs cluster size (stability patterns) at four different temperatures.

It is customary to look at the relative energy stability of the clusters with respect to their neighbors by calculating the second difference of the binding energy at zero temperature. At finite temperatures, it is the second difference of the vibrational free energies $\Delta F_N = F_{N+1} + F_{N-1} - 2F_N$ which indicates the relative structural stability of a cluster. We predict that several highly symmetric clusters become more stable at finite temperatures and fundamentally change the pattern of stability as a function of temperature. Figure 5 shows the temperature changes of ΔF_N as a function of size (stability pattern). The $T=0$ data contains the zero point energy of the clusters which is typically very small, about 0.01 eV for the larger sizes. As clearly seen in Fig. 5, there are some cluster sizes that become quite dominant at higher temperatures. Such is the case of Sr_{34} and Sr_{61}. These sizes are dramatically preferred in the experiment. As the spectrum in Fig. 2 illustrates, there is practically zero abundance at Sr_{35} and Sr_{62} indicating that these cluster sizes are very unstable. Therefore, Sr_{34} and Sr_{61} are distinct magic numbers that have not been observed for other elements.

Looking more closely to the $N=61$ cluster, we find that as in the case of Sr_{34}, Sr_{61} undergoes a structural transition from the C_{2v} structure to a T_d structure at 220 K. Figure 6 illustrates the two structures of Sr_{61} and the change in the internal energy that takes place at the transition. Figures 7(a) and 7(b) show the abrupt change of the entropy and vibrational specific heat when the structural transition takes place. These transitions are driven by the low frequency modes that the high temperature isomers have. Illustrated in Fig. 8 are the frequency spectra of normal modes of both the global minimum at $T=0$ and the high temperature preferred isomer at higher temperatures of Sr_{34} and Sr_{61}. In both cases a broadening of the band is observed at finite temperature, accompanied by a much denser band at low frequencies. The overall effect of temperature is to smear the region of high spectral density in the center of the band, pushing modes towards the band ends. In turn the low frequency modes contribute the most to decrease the free energy at finite tem-

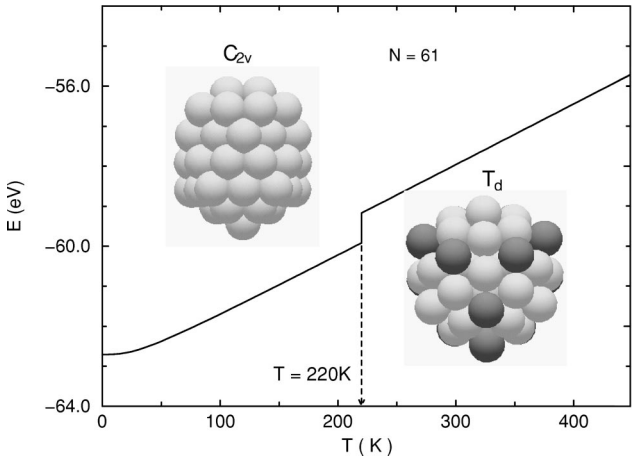

FIG. 6. (a) Internal energy of Sr_{61} as a function of temperature. The global minimum C_{2v} is depicted at low temperatures. The higher energy isomer T_d is depicted at higher temperatures.

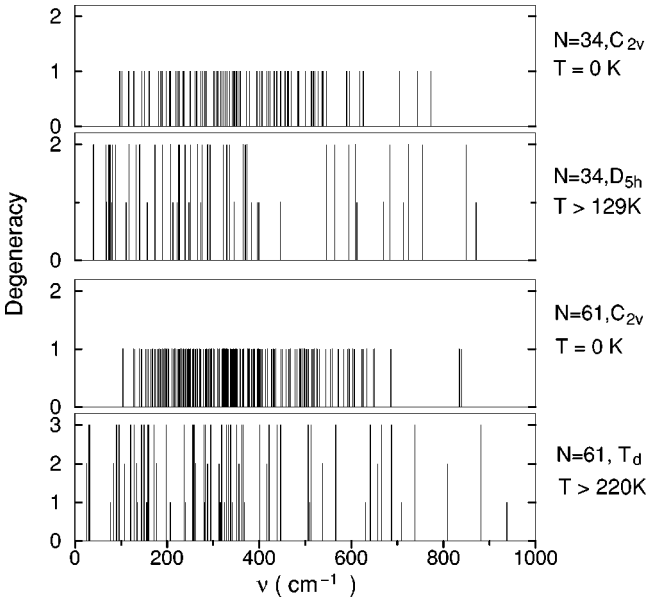

FIG. 8. Normal mode frequencies of the lower energy isomers of Sr_{34} and Sr_{61} at $T=0$ and at finite temperatures.

peratures. Almost all cluster sizes in the range studied here undergo structural transitions at various temperatures below melting. That information is taken into account in Fig. 5. The only cluster sizes that do not transform structurally are 18–20, 22–23, 25–31, 35, 50, 54, and 58–59.

Additionally, several molecular dynamics simulations of a fast cooling process were carried out. This was done to simulate the rapid cooling that takes place in an evaporative process such as that encountered in the experiment described in Sec. V. Clusters were equilibrated at about 400 K for a million time steps, and then quenched to low temperatures. Figure 9 shows the results for ten quenching experiments of Sr_{34} and four experiments for Sr_{61}. Points correspond to averages over 3000 time steps after an equilibration stage of 2000 steps at the desired temperature. As expected, the internal energy as a function of temperature displays two distinct cooling branches. In one the system reaches the most stable cluster at zero temperature (C_{2v} for Sr_{34} and Sr_{61}) and the other branch reaches the most stable cluster above T_s (D_{5h} for Sr_{34} and T_d for Sr_{61}) that has been quenched due to the fast cooling process. These simulations confirm that for selected cluster sizes there are two dynamically preferred structures, i.e., the global minimum structure at temperatures close to the zero point energy and another structure revealed only above the structural transition temperature.

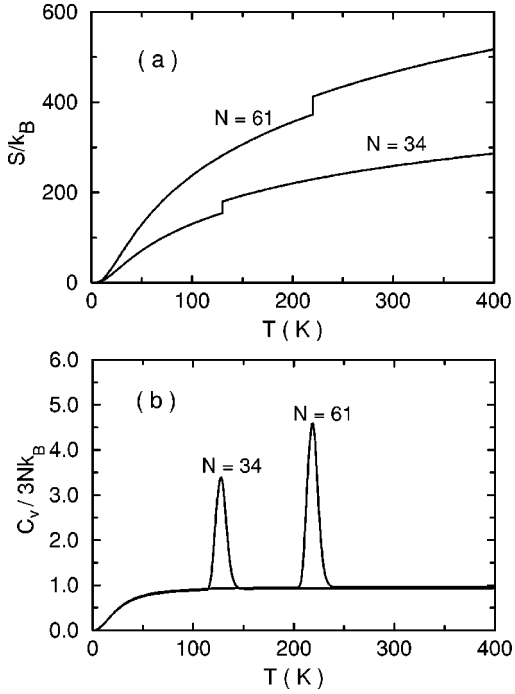

FIG. 7. Thermodynamic functions for Sr_{34} and Sr_{61} as a function of temperature: (a) entropy, (b) specific heat of vibration.

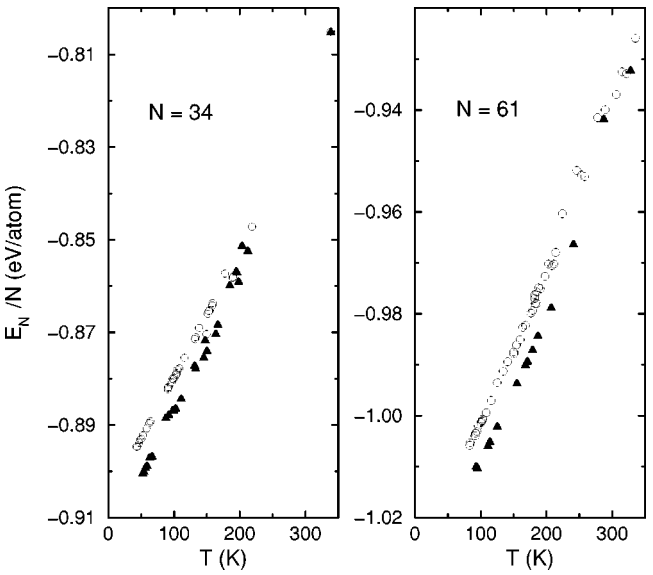

FIG. 9. Total energy as a function of temperature along the cooling process for Sr_{34} and Sr_{61}. Dark triangles refer to quenches that ended in the global minimum structure and circles correspond to quenches that drove the system to the preferred structure above the structural transition temperature.

VII. CONCLUSIONS

The proposed many-body potential for strontium clusters allow for an investigation of the cluster structures up to $N=63$. Results on the energetic stability of clusters in this size range indicate a strong effect of temperature on the magic numbers (more stable sizes). The stability patterns change as the temperature is increased as shown in Fig. 5. At finite temperatures our calculation predicts the magic numbers 34 and 61 of the high resolution mass spectrum reported in Sec. V. The rest of the pattern at 400 K is also in good agreement with the mass spectrum. At cluster sizes 34 and 61, as well as in others, we predict structural transitions from the isomer corresponding to the global minimum transforming into a more spherelike higher energy isomer. These transitions take place at temperatures below 500 K and are driven by the low frequency modes of the structures. Specifically, the C_{2v} clusters Sr_{34} and Sr_{61} undergo a structural transition to the D_{5h} and T_d symmetries, respectively. It is important to note that the entropy of Sr_{34} and Sr_{61} increases with temperature, presents a discontinuity at the structural transition temperature, and shows that the high temperature stable structures have significantly larger entropy [Fig. 7(a)]. The structural transition, however, is driven by the important contribution of the low frequency vibrational modes to the free energy F at finite temperatures. Since the clusters are assumed to be in thermal equilibrium at a temperature T, the entropy S is obtained from the free energy as $S(T)=[E(T)-F(T)]/T$. Therefore, it is the change in the structural stability of the cluster evidenced by its free energy that drives the structural transitions.

In this work we also report hybrid GGA calculations for Sr clusters with up to 10 atoms. These first principles results allow us to fit the parameters of the many-body potential. From the study at zero temperature we then predict the trend of the binding energy as the cluster size increases. A comparison to the MM and Morse potentials parametrized for strontium shows that both of these potentials give a different trend of how the binding energy as a function of size reaches the bulk value.

No experiments exist today concerning the structure of strontium clusters, probably because strontium is a very reactive element and combines readily with oxygen. Therefore pure Sr clusters are challenging systems for experimental findings. In this direction the predictive content of this work should be helpful.

ACKNOWLEDGMENTS

The authors are grateful to Professor Kenneth A. De Jong for enlighting us with his method of multiple point crossover which proved to be fundamental in the optimization process. One of the authors (E.B.B.) acknowledges partial support from Grant No. CTS-9806321 of the National Science Foundation.

[1] S. Sugano and H. Koizumi, *Microcluster Physics* (Springer-Verlag, New York, 1998).
[2] For example, papers in *Theory of Atomic and Molecular Clusters*, edited by J. Jellinek (Springer-Verlag, New York, 1999).
[3] Y. Li, E. Blaisten-Barojas, and D. Papaconstantopoulos, Phys. Rev. B **57**, 15519 (1998).
[4] T. P. Martin, T. Bergmann, H. Goehlich, and T. Lange, Chem. Phys. Lett. **176**, 343 (1991).
[5] T. P. Martin, U. Naeher, T. Bergmann, H. Goehlich, and T. Lange, Chem. Phys. Lett. **183**, 119 (1991).
[6] T. P. Martin, Phys. Rep. **273**, 199 (1996).
[7] H. Olijnyk and W. B. Holzapfel, Phys. Lett. A **100**, 191 (1984).
[8] R. O. Jones, J. Chem. Phys. **71**, 1300 (1979).
[9] Y. Wang, H-J. Flad, and M. Dolg, J. Phys. Chem. A **104**, 5558 (2000).
[10] J. E. Hearn and R. L. Johnston, J. Chem. Phys. **107**, 4674 (1997).
[11] J. N. Murrell and R. E. Mottram, Mol. Phys. **69**, 571 (1990).
[12] G. Gerber, R. Möller, and H. Schneider, J. Chem. Phys. **81**, 1538 (1984).
[13] P. Dugourd, J. Chevalegre, C. Bordas, and M. Broyer, Chem. Phys. Lett. **193**, 539 (1992).
[14] L. A. Heinebrödt, Ph.D. thesis of Universität Stuttgart, 1999.
[15] C. Bréchignac, Ph. Cahuzac, K. Kebaili, J. Leygnier, and H. Yoshida, Phys. Rev. B **61**, 7280 (2000).
[16] C. H. Chien, E. Blaisten-Barojas, and M. Pederson, J. Chem. Phys. **112**, 2301 (2000).
[17] J. A. Niesse and H. R. Mayne, J. Comput. Chem. **18**, 1233 (1997).
[18] J. Mirick, C.-H. Chien, and E. Blaisten-Barojas, Phys. Rev. A **63**, 023202 (2001).
[19] D. A. Papaconstantopoulos, *Handbook of Band Structure of Elemental Solids* (Plenum, New York, 1986).
[20] V. L. Sliwko, P. Mohn, K. Schwarz, and P. Blaha, J. Phys.: Condens. Matter **8**, 799 (1996).
[21] D. J. Wales, L. J. Munro, and J. P. K. Doye, J. Chem. Soc. Dalton Trans. **1996**, 611.
[22] J. P. K. Doye and D. J. Wales, J. Chem. Soc., Faraday Trans. **93**, 4233 (1997). See also http://www-wales.ch.cam.ac.uk/~jon/structures/Morse.html
[23] F. Cyrot-Lackmann, J. Phys. Chem. Solids **29**, 1235 (1968).
[24] D. G. Pettifor, Solid State Phys. **40**, 43 (1987).
[25] Ch. Kittel, *Introduction to Solid State Physics*, 6th ed. (Wiley, New York, 1986).
[26] F. R. de Boer, R. Boom, W. C. M. Mattens, A. A. R. Miedema, and A. K. Niessen, *Cohesion of Metals* (North–Holland, Amsterdam, 1988).
[27] *Smithells Metals Reference Book*, 6th ed., edited by E. A. Brands (Butterworths, Boston, 1983), pp. 15–16.
[28] J. P. Perdew, J. A. Chevary, S. H. Vosko, K. A. Jackson, M. R. Pederson, D. J. Singh, and C. Fiolhais, Phys. Rev. B **46**, 6671 (1992).
[29] A. D. Becke, J. Chem. Phys. **98**, 5648 (1993).
[30] M. Kaupp, P. V. R. Schleyer, H. Stoll, and H. Preuss, J. Chem. Phys. **94**, 1360 (1991).
[31] M. J. Frisch, G. W. Trucks, H. B. Schlegel *et al.*, GAUSSIAN 98 (Gaussian Inc., Pittsburgh, PA, 1998).
[32] C. J. Tsai and K. D. Jordan, J. Phys. Chem. **97**, 11227 (1993).
[33] S. Kirkpatrick, C. D. Gelatt Jr., and M. P. Vecchi, Science **220**, 671 (1983).
[34] A. E. Roitberg and R. Elber, J. Chem. Phys. **95**, 9277 (1991).
[35] D. J. Wales and H. A. Scheraga, Science **285**, 1368 (1999), and references therein.
[36] F. H. Stillinger and T. A. Weber, Phys. Rev. A **25**, 978 (1982).
[37] D. Goldberg, *Genetic Algorithms in Search, Optimization, and Learning* (Addison–Wesley, MA, 1989).
[38] R. Judson, in *Reviews of Computational Chemistry*, edited by K. B. Lipkowitz and D. B. Boyd (VCH, New York, 1997), Vol. 10, pp. 1–73.
[39] J. Mestres and G. E. Scuseria, J. Comput. Chem. **16**, 729 (1995).
[40] J. A. Niesse and H. R. Mayne, J. Chem. Phys. **105**, 4700 (1996).
[41] D. M. Deaven, N. Tit, J. R. Morris, and K. M. Ho, Chem. Phys. Lett. **256**, 195 (1996).
[42] S. K. Gregurich, M. H. Alexander, and B. Hartke, J. Chem. Phys. **104**, 2684 (1996).
[43] G. W. Turner, E. Tedesco, K. D. M. Harris, R. L. Johnston, and B. M. Kariuki, Chem. Phys. Lett. **321**, 183 (2000).
[44] W. M. Spears and K. A. De Jong, in *Proceedings of the Fourth International Conference on Genetic Algorithms (ICGA-91)*, edited by R. K. Belew and L. B. Booker (Morgan Kaufmann, San Diego, 1991), pp. 230–234.
[45] D. J. Wales and J. P. K. Doye, J. Phys. Chem. A **101**, 5111 (1997). See also http://wwwwales.ch.cam.ac.uk/~jon/structures/LJ.html
[46] J. P. K. Doye and D. J. Wales, New J. Chem. **22**, 733 (1998). See also http://wwwwales.ch.cam.ac.uk/~jon/structures/SC.html